Published OnlineFirst September 25, 2013; DOI: 10.1158/0008-5472.CAN-12-4258

Cancer Research

Targeting Sonic Hedgehog-Associated Medulloblastoma through Inhibition of Aurora and Polo-like Kinases

Shirley L. Markant, Lourdes Adriana Esparza, Jesse Sun, et al.

Cancer Res 2013;73:6310-6322. Published OnlineFirst September 25, 2013.

Published OnlineFirst September 25, 2013; DOI: 10.1158/0008-5472.CAN-12-4258

Tumor and Stem Cell Biology

Cancer Research

Targeting Sonic Hedgehog-Associated Medulloblastoma through Inhibition of Aurora and Polo-like Kinases

Shirley L. Markant[1,2,7], Lourdes Adriana Esparza[1,2], Jesse Sun[7,8], Kelly L. Barton[7,9], Lisa M. McCoig[7], Gerald A. Grant[9,10], John R. Crawford[3,4,6], Michael L. Levy[5,6], Paul A. Northcott[11,12], David Shih[12], Marc Remke[12], Michael D. Taylor[12], and Robert J. Wechsler-Reya[1,2,7]

Abstract

Medulloblastoma is the most common malignant brain tumor in children. Although aggressive surgery, radiation, and chemotherapy have improved outcomes, survivors suffer severe long-term side effects, and many patients still succumb to their disease. For patients whose tumors are driven by mutations in the sonic hedgehog (SHH) pathway, SHH antagonists offer some hope. However, many SHH-associated medulloblastomas do not respond to these drugs, and those that do may develop resistance. Therefore, more effective treatment strategies are needed for both SHH and non-SHH–associated medulloblastoma. One such strategy involves targeting the cells that are critical for maintaining tumor growth, known as tumor-propagating cells (TPC). We previously identified a population of TPCs in tumors from *patched* mutant mice, a model for SHH-dependent medulloblastoma. These cells express the surface antigen CD15/SSEA-1 and have elevated levels of genes associated with the G_2–M phases of the cell cycle. Here, we show that $CD15^+$ cells progress more rapidly through the cell cycle than $CD15^-$ cells and contain an increased proportion of cells in G_2–M, suggesting that they might be vulnerable to inhibitors of this phase. Indeed, exposure of tumor cells to inhibitors of Aurora kinase (Aurk) and Polo-like kinases (Plk), key regulators of G_2–M, induces cell-cycle arrest, apoptosis, and enhanced sensitivity to conventional chemotherapy. Moreover, treatment of tumor-bearing mice with these agents significantly inhibits tumor progression. Importantly, cells from human patient-derived medulloblastoma xenografts are also sensitive to Aurk and Plk inhibitors. Our findings suggest that targeting G_2–M regulators may represent a novel approach for treatment of human medulloblastoma. *Cancer Res; 73(20); 6310–22. ©2013 AACR.*

Introduction

Medulloblastoma is the most common malignant pediatric brain tumor, with the majority of cases occurring in children under the age of 15 years (1). Patients with medulloblastoma are commonly treated with surgery, radiation, and chemotherapy, but survivors suffer severe side effects, including cognitive and developmental deficits and an increased risk of secondary tumors later in life (2, 3). Therefore, alternative approaches to treatment of medulloblastoma are essential.

Recent genomic analyses have identified four major subtypes of medulloblastoma that differ from one another in terms of gene expression, DNA copy number and mutations, epidemiology, and prognosis. Although the genetic drivers of these subtypes are not fully understood, one group of tumors—representing approximately 25% of medulloblastoma cases—is characterized by activation of the sonic hedgehog (SHH) signaling pathway. In some cases, this activation can be attributed to mutation or amplification of known pathway components, including the membrane proteins Patched (PTCH1) and Smoothened (SMO), the cytoplasmic regulator Suppressor of Fused (SUFU), and the transcription factors GLI1 and GLI2; however, in many cases, the basis for SHH pathway activation remains unclear (4).

Patients with SHH-associated tumors have a variable prognosis, with a subset faring poorly despite aggressive therapy (4). The development of small-molecule inhibitors of the SHH pathway has offered some hope for these patients (5, 6). These agents represent one of the first classes of targeted therapies for medulloblastoma, but they are effective only in patients with SHH-associated tumors. Importantly, most of these compounds act on SMO and are thus unlikely to be active against

Authors' Affiliations: [1]Tumor Initiation and Maintenance Program, National Cancer Institute (NCI)–Designated Cancer Center, Sanford-Burnham Medical Research Institute; [2]Sanford Consortium for Regenerative Medicine; Departments of [3]Pediatrics, [4]Neurosciences, and [5]Neurosurgery, University of California San Diego, La Jolla; [6]Rady Children's Hospital, San Diego, California; Departments of [7]Pharmacology and Cancer Biology, [8]Medicine, Division of Pulmonary, Allergy, and Critical Care, [9]Pediatrics, Division of Pediatric Hematology/Oncology, and [10]Surgery, Duke University Medical Center, Durham, North Carolina; [11]German Cancer Research Center (DKFZ), Heidelberg, Germany; and [12]Hospital for Sick Children, University of Toronto, Toronto, Ontario, Canada

Note: Supplementary data for this article are available at Cancer Research Online (http://cancerres.aacrjournals.org/).

Corresponding Author: Robert J. Wechsler-Reya, Tumor Initiation and Maintenance Program, National Cancer Institute (NCI)–Designated Cancer Center, Sanford-Burnham Medical Research Institute, 2880 Torrey Pines Scenic Drive, La Jolla, CA 92037. Phone: 858-795-5115; Fax: 858-534-9250; E-mail: rwreya@sanfordburnham.org

doi: 10.1158/0008-5472.CAN-12-4258

Published OnlineFirst September 25, 2013; DOI: 10.1158/0008-5472.CAN-12-4258

tumors driven by mutations in downstream components such as SUFU and GLI (7). Moreover, recent studies in both patients and animals have shown that PTCH- and SMO-driven tumors that initially respond to SHH antagonists quickly develop resistance (6, 8). Thus, more innovative approaches to therapy are required for SHH-associated medulloblastoma.

One approach for improving treatment of medulloblastoma may involve targeting tumor-propagating cells (TPC). TPCs, often called cancer stem cells, are operationally defined as the cells within a tumor that are capable of regenerating the tumor upon transplantation into a naïve host. TPCs have been identified in multiple tumor types, including those of the brain, breast, prostate, colon, pancreas, liver, lung, and skin, among others (9–16). The ability of TPCs to regenerate tumors has led to the notion that these cells are responsible for tumor resistance and recurrence after therapy. Indeed, TPCs have been shown to display resistance to both chemotherapy and radiation (17–19). Given this capacity for evading standard therapies and regenerating tumors, identification of therapeutic approaches to target and eliminate these cells could substantially improve patient outcomes.

We recently identified a population of TPCs in *patched* heterozygous mice, a widely studied mouse model of SHH-associated medulloblastoma (20). These cells, which can be identified on the basis of their expression of the cell surface carbohydrate antigen CD15/SSEA-1, are not multipotent and cannot form neurospheres, but are uniquely capable of propagating tumors following transplantation. When $CD15^+$ cells are transplanted into the cerebella of naïve mice, 100% of recipients develop tumors, whereas $CD15^-$ cells never generate tumors. Expression profiling revealed that $CD15^+$ cells display decreased expression of genes associated with differentiation and elevated expression of genes associated with proliferation. CD15 is also found in a subset of human medulloblastomas, and patients whose tumors express high levels of a CD15-associated gene signature have a poorer prognosis.

Because $CD15^+$ cells are critical for tumor propagation, we hypothesized that further understanding the properties of these cells might enable us to identify vulnerabilities that could be targeted by therapeutic intervention. Here, we report that $CD15^+$ cells from *patched* mutant tumors display elevated expression of genes encoding regulators of G_2 and M phases of the cell cycle and a corresponding over-representation of cells in G_2–M phase. Furthermore, inhibition of Aurora kinases (Aurk) or Polo-like kinases (Plk), important G_2–M regulators, inhibits proliferation *in vitro* and blocks tumor growth *in vivo*. Therefore, targeting TPCs through inhibition of G_2–M regulators may represent a novel approach for improving treatment of patients with this disease.

Materials and Methods

Mice

All animal experiments were done according to protocols approved by the Institutional Animal Care and Use Committees of Duke University (Durham, NC) and the Sanford-Burnham Medical Research Institute (La Jolla, CA). Germline *patched* heterozygous mutant mice (21) were maintained by breeding with 129×1/SvJ or C57BL/6 mice from The Jackson Laboratory. Conditional Math1-CreER; $Ptc^{flox/flox}$ mice (22) were treated with 0.8 mg of tamoxifen (T5648; Sigma) in 40 μL of corn oil at postnatal day 4 to generate tumors 10 to 16 weeks later. CD-1 Nu/Nu mice were obtained from Charles River Laboratories, and NOD.Cg-*Prkdc*^{scid} *Il2rg*^{tm1Wjl}/SzJ (NOD/scid/gamma; NSG) mice were obtained from The Jackson Laboratory.

Human tumor isolation and propagation

Human medulloblastoma tissue for patient-derived xenografts was obtained from surgical resection of tumors at Duke University Medical Center (Durham, NC) or Rady Children's Hospital (San Diego, CA). All procedures using human tissue were approved by the Institutional Review Boards of the respective institutions. Upon retrieval, the tissue was mechanically dissociated into a single-cell suspension, then immediately injected into the cerebella of NSG mice. When the mice became symptomatic, the tumors were again dissociated into single-cell suspensions and then retransplanted back into the cerebella of naïve hosts to establish a propagated line for each patient-derived xenograft.

Molecular classification of human tumors

The tumors were assigned molecular subgroups using a class prediction algorithm, prediction analysis for microarrays (PAM; ref. 23), as implemented in the pamr R package (v 1.51). The RNA expressions of subgroup-specific markers were measured by a NanoString assay (24) and subsequently used as features for class prediction. Predicted subgroups with confidence probabilities higher than established thresholds (24) were considered *bona fide* subgroup assignments. Principal component analyses (PCA) plots were generated by PCA on the training data. The resulting Eigen vectors were used to project the expression profiles of the classified samples onto the vector space spanned by the first two Eigen vectors of the training data. The background confidence score gradient was generated using 200 replicates of the training data with Gaussian noise and subsequently smoothed by Nadaraya-Watson normalization (fields v6.7.6 R package).

Chemicals

The Aurk inhibitors VX-680, PHA-739358, SNS-314, CYC116, AT9283, MLN8237, PHA-680602, CCT129202, ENMD-2076, and AZD1152-HQPA, the Plk inhibitors BI-2536, BI-6727, GSK461364, and ON-01910, and the chemotherapeutic agents vincristine, cisplatin, and cyclophosphamide were obtained from Selleck Chemicals. The SHH antagonist NVP-LDE225 was kindly provided by Novartis.

Tumor cell isolation and culture

Tumors were obtained from germline *patched* heterozygous or conditional Math1-CreER; $Ptc^{flox/flox}$ mice, and each experiment was done multiple times using cells isolated from each strain. The complete tumor dissociation procedure has been described previously (20, 22). Briefly, tumors were digested in a papain solution to obtain a single-cell suspension, then centrifuged through a 35% to 65% Percoll gradient. Cells from

Published OnlineFirst September 25, 2013; DOI: 10.1158/0008-5472.CAN-12-4258

the 35% to 65% interface were suspended in Dulbecco's PBS (DPBS) plus 5% FBS for cell sorting or in NB-NS21 [Neurobasal with 1 mmol/L sodium pyruvate, 2 mmol/L L-glutamine, penicillin/streptomycin, and NS-21 supplement (25)] plus 1% FBS (Invitrogen) for culture. The cells were plated on Growth Factor–Reduced Matrigel (BD Biosciences)–coated plates.

Cell sorting

To obtain $CD15^+$ and $CD15^-$ cell populations, cells were stained with control mouse immunoglobulin M (IgM) or anti-CD15 (clone MMA; BD Biosciences) antibodies, followed by anti-mouse IgM–phycoerythrin (PE; Jackson ImmunoResearch). The cells were then sorted on a FACSVantage or FACSVantage SE DiVa flow cytometer (BD Biosciences). After sorting, the cells were pelleted and resuspended in NB-NS21 culture media or frozen until use for expression analysis.

Real-time PCR

Real-time PCR was conducted to examine the mRNA expression levels of *AurkA*, *AurkB*, and *Plk1* in the $CD15^+$ and $CD15^-$ populations. mRNA was prepared using an RNeasy kit (Qiagen, Inc.), and real-time PCR was conducted using the QuantiTect SYBR Green RT-PCR Kit (Qiagen, Inc.). Each reaction consisted of 10 ng of the appropriate RNA, 12.5 μL of 2× QuantiTect SYBR Green RT-PCR Master Mix, 1.25 μL of a 10 μmol/L stock of the appropriate forward and reverse primers, 0.25 μL of QuantiTect RT mix, and RNase-free water in a total volume of 25 μL. The following primer sequences were used: AurkA, forward: GTTCCCTTCGGTCCGAAA, reverse: AATCATTTCCGGAGGCTG; AurkB, forward: TCAGAAGGAGAACGCCTACCC, reverse: GACTCTCTGGGACAACGTGTT; Plk1, forward: ACGTCGTAGGCTTCCATGAC, reverse: CTCGTTCAGGAAGAGGTTGC; and Actin, forward: TATTGGCAACGAGCGGTTCC, reverse: GGCATAGAGGTCTTTACGGATGTC. Duplicate reactions were carried out without the QuantiTect RT mix to confirm the absence of genomic DNA contamination. The following reaction conditions were run on a Bio-Rad C1000 Thermal Cycler and CFX96 Real-time System (Bio-Rad Laboratories): reverse transcription at 50°C for 30 minutes, HotStarTaq DNA Polymerase activation at 95°C for 15 minutes, followed by 40 cycles of 94°C for 15 seconds, 60°C for 30 seconds, and 72°C for 30 seconds. Each reaction was analyzed in triplicate using the ΔC_t method to determine the level of expression of each gene in the $CD15^+$ population relative to the $CD15^-$ population in each tumor.

BrdUrd and cell-cycle analysis

To monitor cell-cycle kinetics, tumor cells were first sorted into $CD15^+$ and $CD15^-$ populations as described earlier. After sorting, 2 million cells per well were plated into 24-well plates in NB-NS21 culture media. The cells were pulsed with bromodeoxyuridine (BrdUrd) for 30 minutes, then washed with media to remove any remaining BrdUrd. Cells were collected immediately after the pulse (30 minutes), or 6, 12, or 24 hours later, then fixed and stained using the fluorescein isothiocyanate (FITC) BrdU Flow Kit (BD Biosciences) and 7-aminoactinomycin (7-AAD) according to the manufacturer's instructions. For cell-cycle analysis of cells that were not labeled with BrdUrd, the same kit was used for fixation, permeabilization, and 7-AAD staining, but the anti-BrdUrd staining step was omited. The analysis was conducted using a FACScan or FACSCanto flow cytometer (BD Biosciences) and FlowJo v.7.6.4 software (TreeStar, Inc.).

CFSE analysis

As an alternative approach to measure the timing of cell divisions in $CD15^+$ and $CD15^-$ populations, *patched* mutant tumor cells were sorted, then labeled with 1 μmol/L carboxyfluorescein diacetate (CFSE) at a density of 1×10^6 cells/mL using the CellTrace CFSE Cell Proliferation Kit (Invitrogen). The cells were then cultured for 48, 72, or 96 hours, fixed with 2% paraformaldehyde (PFA), and CFSE fluorescence was analyzed using a FACSCanto flow cytometer (BD Biosciences) and FlowJo v.7.6.4 software (TreeStar, Inc).

Western blotting

To assess the levels of histone H3 phosphorylation following treatment with inhibitors, cells were cultured in 24-well plates at a density of 2.5 million cells per well in the presence of the indicated concentrations of DMSO, VX-680, or BI-2536. Cells were then lysed in radioimmunoprecipitation assay buffer (Millipore) containing 1 mmol/L sodium orthovanadate, 2 mmol/L sodium fluoride (both from Sigma), and complete, mini, EDTA-free protease inhibitor tablets (Roche Applied Science). Proteins (30 μg) were resolved by SDS-PAGE and transferred to nitrocellulose membranes (Invitrogen), which were then probed with antibodies against phospho-histone H3 (Ser 10; Millipore), total histone H3 (Cell Signaling Technology), actin (Santa Cruz Biotechnology), or glyceraldehyde-3-phosphate dehydrogenase (GAPDH; Cell Signaling Technology), followed by goat anti-rabbit antibodies conjugated to IRdye 680 (Rockland). Proteins were detected using the Odyssey imaging system (LI-COR).

Proliferation and apoptosis assays

To examine the effects of inhibitors on proliferation, tumor cells from *patched* mutant mice or patient-derived xenografts were isolated as described earlier and plated in 96-well plates at a density of 0.2 million cells per well. Cells were cultured in the presence of the indicated concentrations of inhibitors for 48 hours in triplicate wells, then pulsed with [methyl-^{3}H]thymidine (Amersham/GE Healthcare) and cultured for an additional 16 to 18 hours. Cells were harvested onto filters using a Mach IIIM Manual Harvester 96 (Tomtec), and incorporated radioactivity was quantified by liquid scintillation spectrophotometry on a Wallac MicroBeta scintillation counter (PerkinElmer).

To measure the effects of inhibitors in combination with radiation, *patched* mutant tumor cells were plated in 96-well plates at a density of 0.2 million cells per well and cultured in the presence of DMSO, 10 nmol/L BI-2536, or 30 nmol/L VX-680. After 24 hours, cells were subjected to 0, 0.25, 0.5, or 1 Gy radiation using a Gammacell 40 Exactor (low-dose cesium 137 irradiator; Best Theratronics Ltd.). The cells were then cultured for an additional 24 hours, and [methyl-^{3}H]thymidine assays were conducted as described earlier.

Published OnlineFirst September 25, 2013; DOI: 10.1158/0008-5472.CAN-12-4258

To determine whether Aurk or Plk inhibitors induce apoptosis *in vitro*, tumor cells from *patched* mutant mice were isolated as described earlier and plated in 48-well plates at a density of 0.5 million cells per well. Cells were cultured in the presence of the indicated concentrations of inhibitors for 48 hours, then collected and suspended in 100 μL of Annexin-binding buffer containing 5 μL of Annexin V–FITC (BD Biosciences). The cells were incubated at room temperature for 15 minutes, 400 μL of Annexin-binding buffer was added, and the percentage of Annexin V–FITC–bound cells was analyzed using a FACSCanto flow cytometer.

In vivo drug administration

To assess the effects of Aurk or Plk inhibition on tumor growth, 8 million cells from *patched* mutant mice were suspended in 50% NB-NS21/50% Growth Factor–Reduced Matrigel and subcutaneously injected in a total volume of 100 μL into the flanks of CD-1 Nu/Nu mice. Tumors were measured using calipers, and tumor volumes were calculated using the formula volume $= 0.52 \times \text{length} \times \text{width}^2$ (26). Drug treatment was initiated when tumors reached a volume of approximately 150 mm^3. Animals were treated with 50 mg/kg BI-2536 (suspended in 0.1 N HCl, then diluted in saline) twice weekly via tail vein. Animals treated with PHA-739358 (30 mg/kg in 5% dextrose) were injected intraperitoneally twice daily. The animals were sacrificed when the largest tumor volume in the cohort exceeded 2 cm^3. After sacrifice, tumors were collected, weighed, and photographed.

To determine whether Plk inhibition induces apoptosis *in vivo*, tumor-bearing mice were treated with a single dose of vehicle or BI-2536, and tumors were harvested 24 hours later and fixed overnight in 4% PFA. After fixation, samples were transferred to a solution of 30% sucrose (Sigma) for 2 days, then embedded in Tissue-Tek optimal cutting temperature compound (Sakura Finetek USA, Inc.). Samples were then stored at −80°C until sectioning (12 μm) on a Leica CM3050S Cryostat (Leica Microsystems, Inc.). For immunostaining, tumor sections were blocked and permeabilized for 1 hour with PBS containing 0.1% Triton X-100 and 1% normal goat serum, stained with anti-cleaved caspase-3 (anti-CC3) antibodies (Cell Signaling Technology) overnight at 4°C, and incubated with Alexa Fluor-594 anti-rabbit IgG (1:200) secondary antibodies for 45 minutes at room temperature. Sections were counterstained with 4′,6-diamidino-2-phenylindole (DAPI; Invitrogen) and mounted with Fluoromount-G (Southern Biotech). Images were acquired using a Zeiss LSM 700 confocal microscope (Carl Zeiss Microscopy, LLC). Quantitation of apoptosis was conducted by acquiring images of six representative regions from four tumors from vehicle-treated mice and four tumors from BI-2536–treated mice and analyzing the number of CC3-positive ($CC3^+$) cells relative to the DAPI-occupied area within each image using Image Pro-Plus 7.0 software (Media Cybernetics, Inc.).

Results

$CD15^+$ cells display elevated expression of G_2–M regulators

To gain insight into the mechanisms underlying tumor propagation by $CD15^+$ cells, we previously compared their gene expression profiles to those of $CD15^-$ cells from the same tumors (20). Our analysis revealed that $CD15^+$ cells express elevated levels of cell-cycle regulators, and in particular, regulators of G_2–M. To validate these data, we analyzed expression of several of these regulators by real-time reverse transcriptase (RT)-PCR. As shown in Fig. 1A–C, expression of *AurkA*, *AurkB*, and *Plk1* was significantly higher in the $CD15^+$ population compared with the $CD15^-$ population in each tumor examined ($n = 3$). These results suggest that $CD15^+$ and $CD15^-$ cells can be distinguished on the basis of their expression of G_2–M regulators.

$CD15^+$ cells are enriched in G_2–M

The differential expression of G_2–M regulators in $CD15^+$ and $CD15^-$ cells suggested that these populations might differ in terms of cell-cycle distribution. To examine this, we conducted cell-cycle analysis on freshly isolated $CD15^+$ and $CD15^-$ cells. Analysis of multiple tumors ($n = 6$) indicated that compared with the $CD15^-$ population, the $CD15^+$ population contains a significantly higher proportion of cells in G_2–M phase; approximately 20% of $CD15^+$ cells reside in G_2–M, compared with approximately 5% of $CD15^-$ cells (Fig. 1D and E). A similar, but less pronounced, enrichment was seen in the proportion of $CD15^+$ cells in S-phase (data not shown). These data suggest that the elevated expression of G_2–M regulators correlates with an increased proportion of $CD15^+$ cells in G_2–M phase.

$CD15^+$ cells progress more rapidly through the cell cycle than $CD15^-$ cells

The increased proportion of $CD15^+$ cells in G_2–M phase could be explained by differences in cell-cycle kinetics between the $CD15^+$ and $CD15^-$ populations. To address this possibility, we pulse-labeled cells with BrdUrd and followed their progression through the cell cycle. $CD15^+$ and $CD15^-$ cells from *patched* mutant tumors were cultured in the presence of BrdUrd for 30 minutes, and then washed and collected immediately for cell-cycle analysis or cultured for an additional 6, 12, or 24 hours. As shown in Fig. 2A and B, BrdUrd was incorporated into both $CD15^+$ and $CD15^-$ cells; approximately 27% of the $CD15^+$ cells incorporated the BrdUrd label, whereas only 7% of the $CD15^-$ cells were labeled. These data suggest that the over-representation of $CD15^+$ cells in G_2–M phase may result, in part, from an increased percentage of cells transiting through the cycle.

To assess the kinetics with which each population proceeds through S-phase and into G_2–M, we examined the ratio of $BrdUrd^+$ cells with 4N DNA (G_2–M phase) to those with DNA content >2N and <4N (S-phase) at each time point (Fig. 2C and Supplementary Fig. S1A–S1E). Thirty minutes after the BrdUrd pulse, the $CD15^+$ and $CD15^-$ populations included similar proportions of cells in S and G_2–M (G_2–M:S ratios = 1.05 and 1.07, respectively). However, as early as 6 hours after the BrdUrd pulse, $CD15^+$ and $CD15^-$ cells began to exhibit differences in cell-cycle distribution. In the $CD15^-$ population, the G_2–M:S ratio increased slowly to 1.24 at 6 hours, 1.45 at 12 hours, and 1.89 at 24 hours. In contrast, this ratio increased much more rapidly in the $CD15^+$ population, reaching 1.92 at 6 hours and 2.42 at 12 hours. At 24 hours, the G_2–M:S ratio in the

Published OnlineFirst September 25, 2013; DOI: 10.1158/0008-5472.CAN-12-4258

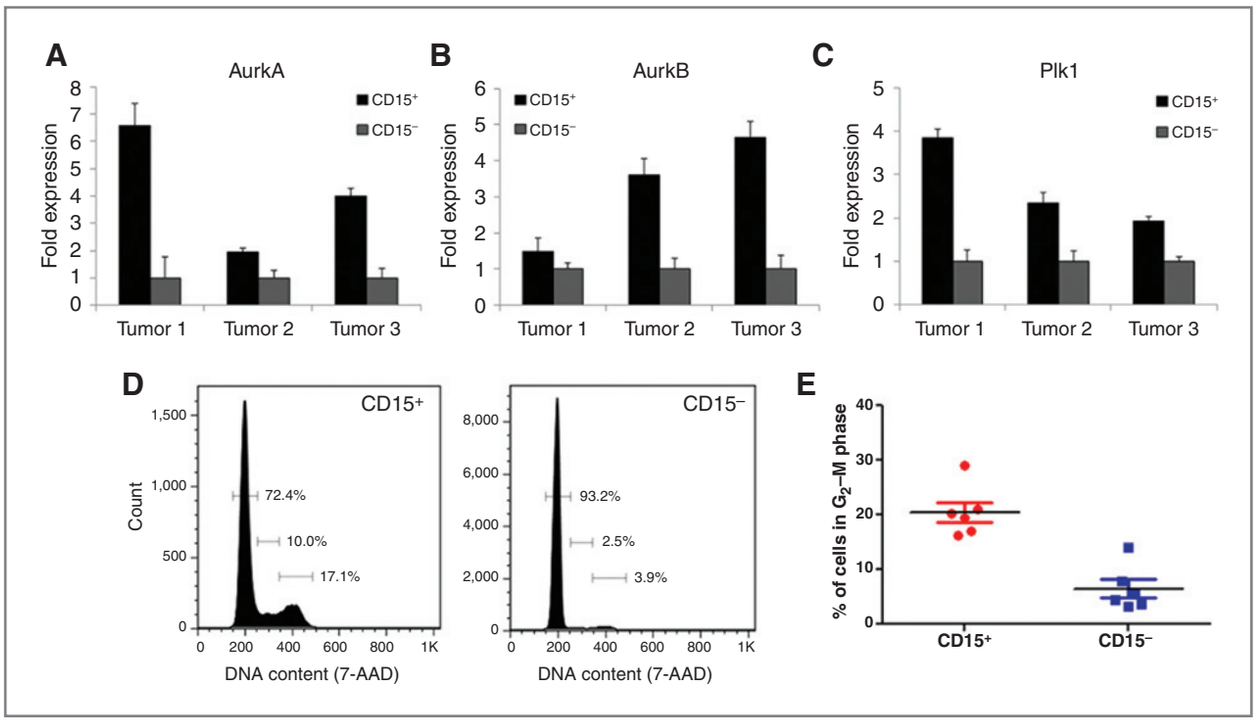

Figure 1. CD15$^+$ cells display elevated expression of Aurk and Plk and an increased proportion of cells in G_2–M. A–C, real-time RT-PCR analysis of *AurkA* (A), *AurkB* (B), and *Plk1* (C) expression in CD15$^+$ cells and CD15$^-$ cells from *patched* mutant tumors ($n = 3$). D, flow cytometric analysis of DNA content in CD15$^+$ and CD15$^-$ cells from a representative tumor. E, quantitation of the percentage of cells in G_2–M phase in the CD15$^+$ and CD15$^-$ populations from six separate tumors.

CD15$^+$ population dropped sharply to 1.3, as many CD15$^+$ cells exited G_2–M and reentered G_1. Thus, CD15$^-$ cells require 24 hours to accumulate in G_2–M phase at levels similar to those reached by the CD15$^+$ cells within 6 hours. On the basis of these results, we conclude that CD15$^+$ cells move through the cell cycle more rapidly than CD15$^-$ cells and that this rapid progression may also contribute to the over-representation of CD15$^+$ cells in G_2–M phase.

As an alternative approach for comparing the cell-cycle kinetics of CD15$^+$ and CD15$^-$ populations, we followed cells after labeling with CFSE. CFSE is equally distributed between daughter cells during division, such that a 50% reduction in fluorescence corresponds to one cell division. Thus, the number of divisions a population of cells has undergone can be determined by counting the number of CFSE fluorescence peaks. As shown in Supplementary Fig. S1F, CD15$^+$ and CD15$^-$ cells incorporated similar levels of the CFSE label at $t = 0$. By comparing the median fluorescence of the last peak (lowest fluorescence) in the CD15$^+$ and CD15$^-$ populations to the peak with the highest fluorescence in the CD15$^-$ population (representing undivided cells) at 48, 72, and 96 hours, we found that the majority of the CD15$^+$ population had undergone more divisions than the CD15$^-$ population at each time point (Supplementary Fig. S1G–S1I). Furthermore, closer inspection of the CFSE fluorescence at 96 hours after labeling revealed that approximately 86% of the CD15$^+$ population had undergone four cell divisions, suggesting an average cell-cycle time of 24 hours (Supplementary Fig. S1J–S1L). In contrast, only 5% of the CD15$^-$ population had undergone four divisions, whereas the remaining cycling cells were relatively equally distributed between one, two, and three divisions, suggesting an average cell-cycle time of 60 hours. Therefore, these data further support the conclusion that the CD15$^+$ population from *patched* mutant tumors contain a greater proportion of cycling cells and that these cells progress through the cell cycle more rapidly than CD15$^-$ cells.

Targeting G_2–M regulators blocks progression through the cell cycle, inhibits proliferation, and induces apoptosis

The increased proportion of CD15$^+$ cells in G_2–M phase led us to hypothesize that *patched* mutant tumors might be sensitive to inhibitors of regulators of G_2–M progression. To address this possibility, we treated tumor cells with the Aurk inhibitor VX-680 (tozasertib) and the Plk inhibitor BI-2536 and examined phosphorylation of histone H3 on serine 10. This residue is a direct target of AurkB (27, 28), and as shown in Fig. 3A, the Aurk inhibitor VX-680 potently blocked its phosphorylation. Paradoxically, inhibitors of Plk1 have been reported to promote increased phosphorylation of histone 3 on serine 10 (29, 30); consistent with this, we observed increased levels of phospho-H3^{Ser10} and decreased levels of serine 46 phosphorylation of TCTP (translationally controlled tumor protein, a direct Plk1 substrate) upon treatment with BI-2536 (Fig. 3B and data not shown). These data suggest that inhibitors of Aurk and Plk are active in *patched* mutant tumor cells.

Published OnlineFirst September 25, 2013; DOI: 10.1158/0008-5472.CAN-12-4258

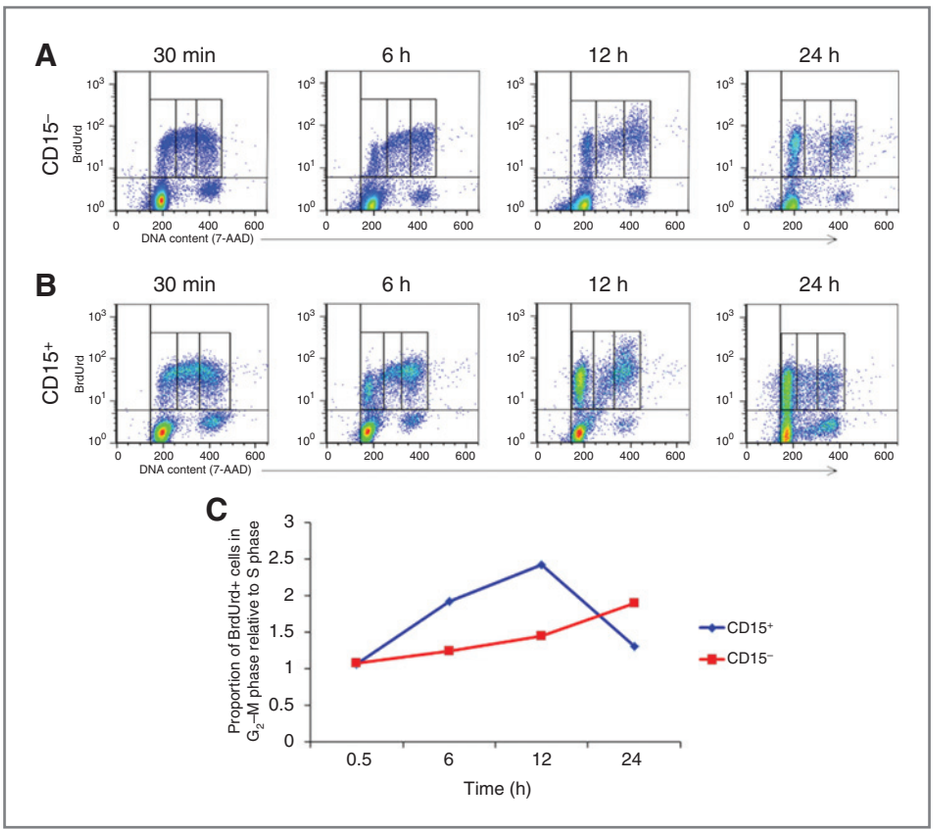

Figure 2. CD15$^+$ cells progress more rapidly through the cell cycle than CD15$^-$ cells. CD15$^+$ and CD15$^-$ cells from germline *patched* mutant tumors were pulsed with BrdUrd for 30 minutes, washed, and then analyzed immediately (30 minutes) or cultured for an additional 6, 12, or 24 hours. A and B, flow cytometric analysis of BrdUrd (*y*-axis) and DNA content (*x*-axis) of CD15$^-$ (A) and CD15$^+$ (B) cells at the indicated time points. C, ratio of (percentage of cells in G_2–M): (percentage of cells in S-phase) among the BrdUrd$^+$ population at each time point. The percentage of CD15$^+$ cells in G_2–M phase increases much more rapidly than the percentage of CD15$^-$ cells in G_2–M between 30 minutes and 12 hours, and CD15$^+$ cells exit G_2–M phase (indicated by drop in the G_2–M to S ratio) sooner than CD15$^-$ cells.

To determine the effects of Aurk and Plk inhibitors on proliferation, we conducted ^{3}H-thymidine incorporation assays. As shown in Fig. 3C, treatment with 100 or 500 nmol/L VX-680 or BI-2536 caused nearly complete inhibition of proliferation. To define the IC_{50} values for VX-680 and BI-2536, we treated cells with increasing concentrations of these compounds (0.15 nmol/L to 1.5 μmol/L) and measured ^{3}H-thymidine incorporation. As shown in Supplementary Fig. S2A and S2B, the IC_{50} values for VX-680 and BI-2536 were 23 and 4.5 nmol/L, respectively. These values are consistent with previously reported IC_{50} values for these drugs in other types of tumor cells (28, 29). To further validate the antiproliferative effects of Aurk and Plk inhibition, we assessed the sensitivity of *patched* mutant tumor cells to additional Aurk or Plk inhibitors. As shown in Supplementary Fig. S2C and S2D, multiple Aurk and Plk inhibitors displayed potent antiproliferative effects. These data confirm that *patched* mutant tumor cells are vulnerable to small molecule–mediated inhibition of Aurk or Plk activity.

To assess the effects of these inhibitors on cell-cycle progression, we treated *patched* mutant tumor cells with VX-680 or BI-2536 for 24 or 48 hours. For comparison, we also treated cells with the SHH antagonist NVP-LDE225 (LDE-225), which is currently in clinical trials for the treatment of SHH-associated medulloblastoma (31). As shown in Fig. 3D and E, exposure to LDE-225 caused a progressive decrease in the number of cells in G_2–M and a concomitant accumulation of cells in G_1. In contrast, both VX-680 and BI-2536 markedly increased the number of cells in G_2–M, and at the same time, decreased the G_1 population (Fig. 3D, F, and G). Treatment with each of these inhibitors also caused an increase in the proportion of cells with <2N DNA, most likely representing apoptotic cells. Consistent with this, VX-680 and BI-2536 each increased the percentage of Annexin V–labeled tumor cells (Fig. 3H). These data suggest that *patched* mutant tumor cells are sensitive to Aurk or Plk inhibition and that the effects of these inhibitors on the cell cycle are distinct from those induced by inhibitors of the SHH pathway.

Plk inhibition cooperates with SHH antagonists and conventional chemotherapy and radiation

Given the distinct effects of LDE-225 and VX-680 or BI-2536 on cell-cycle progression, we hypothesized that these drugs might exert complementary or cooperative effects. To address this possibility, we treated tumor cells with increasing concentrations (0.15–1,500 nmol/L) of LDE-225 either with or without 10 nmol/L BI-2536, a concentration of BI-2536 that caused minimal inhibition of proliferation on its own. As shown in Fig. 4A, treatment with LDE-225 alone inhibited proliferation at concentrations above 15 nmol/L, with an IC_{50} of approximately 9 nmol/L. However, concomitant treatment with 10 nmol/L BI-2536 enhanced the inhibition of proliferation at all concentrations of LDE-225 and caused the IC_{50} for LDE-225 to shift to approximately 2 nmol/L, suggesting that BI-2536 cooperates with LDE-225 to inhibit proliferation. Similar cooperation was observed between VX-680 and LDE-225 (Supplementary Fig. S3A).

Published OnlineFirst September 25, 2013; DOI: 10.1158/0008-5472.CAN-12-4258

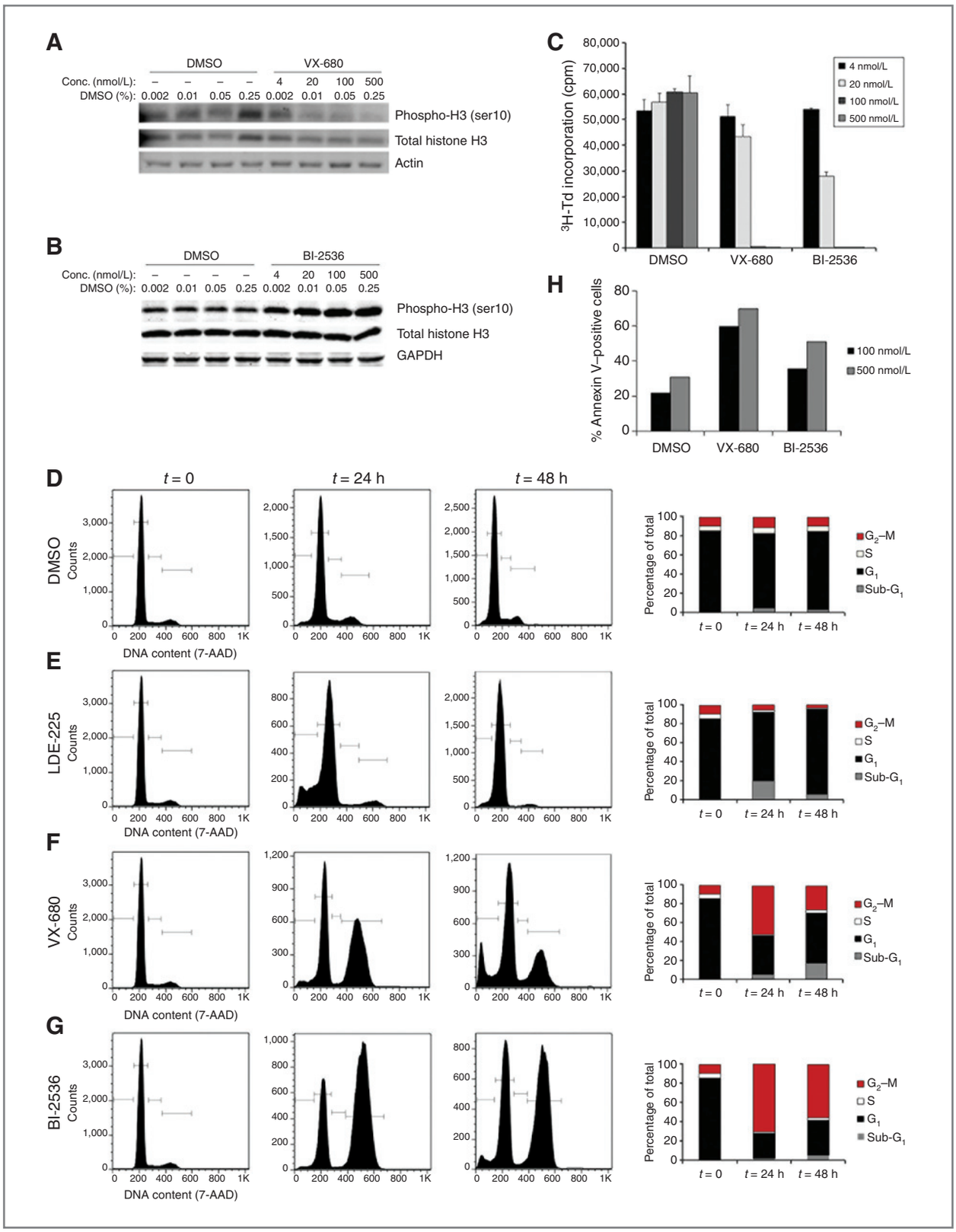

Figure 3. Aurk and Plk inhibitors block proliferation and cell-cycle progression and induce apoptosis. Cells from conditional *patched* mutant tumors were cultured in the presence of the indicated concentrations of VX-680, BI-2536, or the corresponding percentages of DMSO. (*Continued on the following page*.)

Published OnlineFirst September 25, 2013; DOI: 10.1158/0008-5472.CAN-12-4258

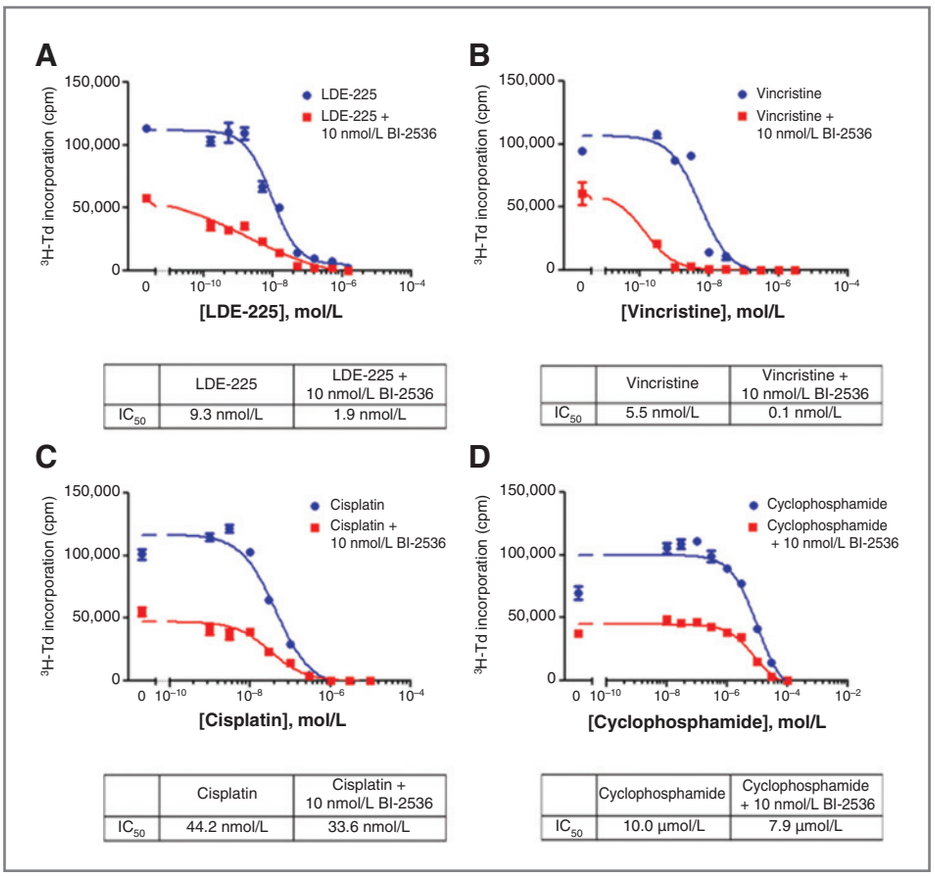

	LDE-225	LDE-225 + 10 nmol/L BI-2536
IC_{50}	9.3 nmol/L	1.9 nmol/L

	Vincristine	Vincristine + 10 nmol/L BI-2536
IC_{50}	5.5 nmol/L	0.1 nmol/L

	Cisplatin	Cisplatin + 10 nmol/L BI-2536
IC_{50}	44.2 nmol/L	33.6 nmol/L

	Cyclophosphamide	Cyclophosphamide + 10 nmol/L BI-2536
IC_{50}	10.0 μmol/L	7.9 μmol/L

Figure 4. Plk inhibitor cooperates with SHH antagonist and chemotherapeutic agents. Conditional *patched* mutant tumor cells were treated with increasing concentrations of the SHH antagonist LDE-225 (A) or the chemotherapeutic agents vincristine (B), cisplatin (C), or cyclophosphamide (D), alone or in combination with 10 nmol/L BI-2536. Cells were cultured for 48 hours, pulsed with ^{3}H-Td, and harvested for analysis of ^{3}H-Td incorporation at 66 hours. Data represent means of triplicate samples ± SEM. IC_{50} values were calculated using the log (inhibitor) vs. response equation [$Y = \text{Bottom} + (\text{Top} - \text{Bottom})/(1 + 10^{(X - \log IC_{50})})$] in GraphPad Prism software.

To determine whether G_2–M inhibitors can also cooperate with conventional chemotherapeutic agents, we treated *patched* mutant tumor cells with 10 nmol/L BI-2536 in combination with vincristine, cisplatin, and cyclophosphamide, chemotherapeutic agents that are currently being used to treat human medulloblastoma (7). Addition of BI-2536 dramatically increased the sensitivity of the tumor cells to vincristine; while the IC_{50} value for vincristine alone was approximately 5 nmol/L, the IC_{50} value for vincristine combined with BI-2536 was approximately 0.1 nmol/L (Fig. 4B). Similar, but less dramatic, cooperation was observed with cisplatin (IC_{50} = 44 nmol/L for cisplatin alone and 34 nmol/L for cisplatin + BI-2536) and with cyclophosphamide (IC_{50} = 10 μmol/L for cyclophosphamide alone and 8 μmol/L for cyclophosphamide + BI-2536; Fig. 4C and D). VX-680 also cooperated with vincristine and cyclophosphamide (Supplementary Fig. S3B–S3D).

To determine whether the G_2–M inhibitors can cooperate with radiotherapy (another component of standard medulloblastoma therapy that is associated with substantial toxicity), we treated *patched* mutant tumor cells with 10 nmol/L BI-2536 or 30 nmol/L VX-680 in combination with increasing doses (0, 0.25, 0.5, and 1 Gy) of radiation. Both BI-2536 and VX-680 significantly enhanced the sensitivity of the cells to radiation (Supplementary Fig. S4A and S4B). These data suggest that the addition of BI-2536 or VX-680 can lower the concentrations of chemo- or radiotherapy required for effective inhibition of tumor cell proliferation.

Inhibition of G_2–M regulators blocks tumor growth *in vivo*

Given the strong antiproliferative effects of the Aurk and Plk inhibitors *in vitro*, we next questioned whether inhibition of G_2–M regulators could affect tumor growth *in vivo*. Because the Plk inhibitor BI-2536 has shown promising results in clinical trials completed thus far (32–34), we prioritized this compound for our *in vivo* studies. *patched* mutant tumor cells were

(*Continued*.) A and B, Western blot analysis of the levels of phospho-histone H3 (Ser10) after 6 hours of treatment with VX-680 (A) or BI-2536 (B). Note that Aurk inhibition decreases phosphorylation, whereas Plk inhibition increases it. C, effects of Aurk and Plk inhibitors on proliferation. Cells were cultured with DMSO, VX-680, or BI-2536, pulsed with tritiated thymidine (^{3}H-Td) at 48 hours, and harvested at 66 hours for analysis of ^{3}H-Td incorporation. Data represent means of triplicate wells ± SEM. Treatment with 20, 100, and 500 nmol/L BI-2536 or VX-680 significantly inhibited ^{3}H incorporation compared with corresponding DMSO controls ($P < 0.01$, based on paired two-tailed *t* test). D–G, flow cytometric analysis of DNA content and graphical representation of percentages of cells in each cell-cycle phase after treatment with DMSO (D), 100 nmol/L LDE-225 (E), 100 nmol/L VX-680 (F), or 100 nmol/L BI-2536 (G). H, effects of Aurk and Plk inhibitors on apoptosis. Cells were cultured with DMSO, VX-680, or BI-2536 for 48 hours, then analyzed for Annexin V–FITC binding. Graph represents percentage of Annexin V–positive cells under each condition in a representative experiment.

Published OnlineFirst September 25, 2013; DOI: 10.1158/0008-5472.CAN-12-4258

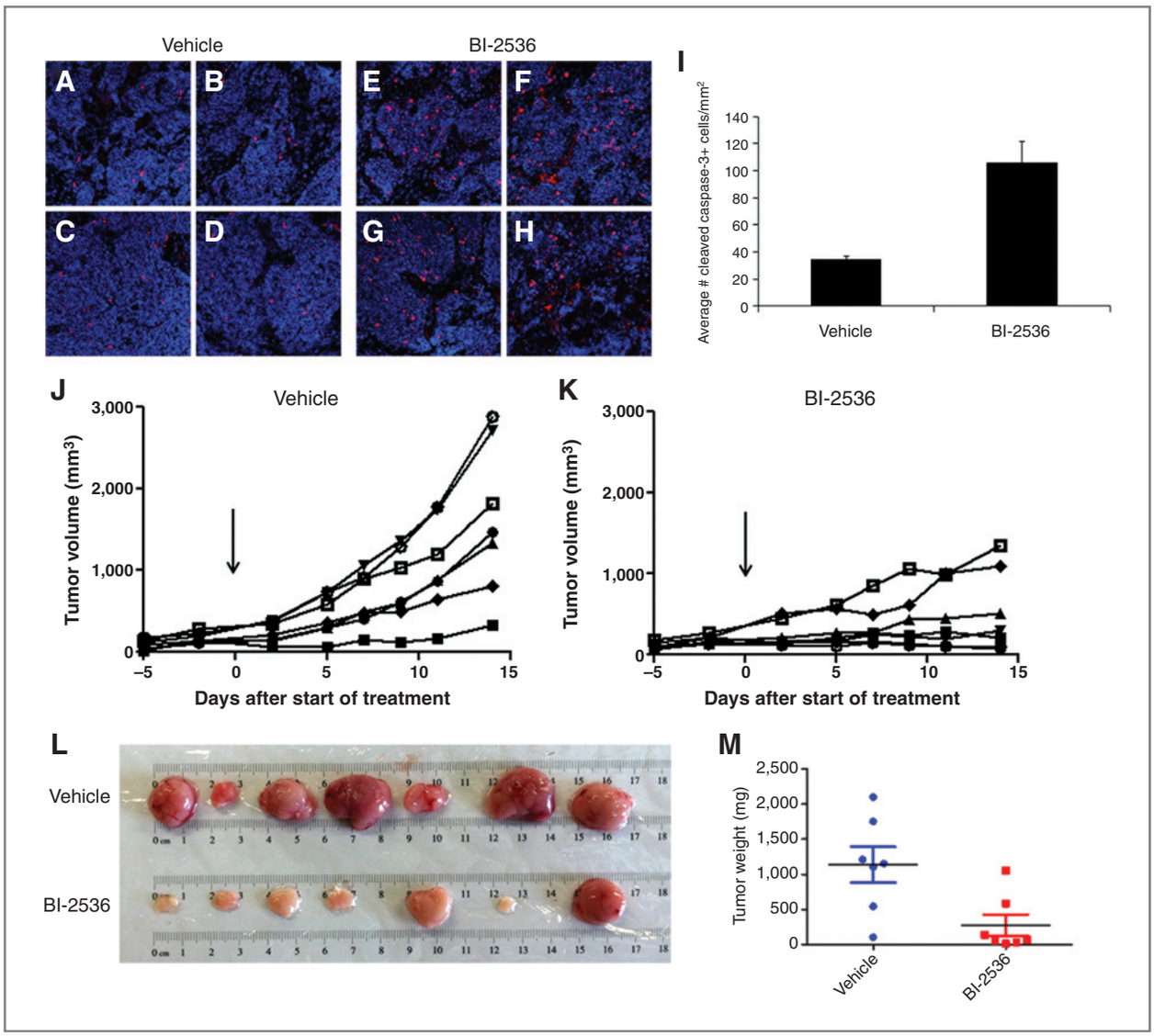

Figure 5. Plk inhibitor induces apoptosis and blocks tumor growth *in vivo*. Mice bearing subcutaneous allografts of conditional *patched* mutant tumor cells were treated twice weekly with vehicle (saline) or 50 mg/kg BI-2536. A–I, twenty-four hours after a single dose of vehicle or BI-2536, tumors were harvested and stained with CC3 antibodies to detect apoptotic cells and DAPI to detect nuclei. Representative images from four independent vehicle-treated (A–D) and BI-2536–treated (E–H) mice are shown. I, $CC3^+$ cells were quantitated and normalized to the DAPI-positive area in six regions from each vehicle-treated and BI-2536–treated tumor. Graph displays the average number of $CC3^+$ cells per mm^2 of DAPI. BI-2536–treated tumors contained significantly more $CC3^+$ cells relative to vehicle-treated tumors ($P = 0.0038$; paired two-tailed *t* test). J and K, tumor volume (mm^3) was measured using calipers. Arrow indicates start of treatment, and each line represents an individual mouse. L, images of tumors. M, tumor weights. Each point represents a single tumor, and gray lines represent mean tumor weights, which were significantly different between vehicle- and BI-2536–treated mice ($P < 0.05$, based on paired two-tailed *t* test).

implanted subcutaneously into the flanks of Nu/Nu mice, and 2 weeks later, mice were treated with either vehicle or BI-2536 (50 mg/kg via tail vein). Tumors were harvested 24 hours later, and sections from four independent tumors per condition were stained with antibodies specific for CC3. As shown in Fig. 5A–I, tumors from BI-2536–treated animals contained significantly more $CC3^+$ cells compared with tumors from vehicle-treated animals (106 $CC3^+$ cells/mm^2 with BI-2536 vs. 34 $CC3^+$ cells/mm^2 with vehicle). These data suggest that treatment with the Plk inhibitor causes apoptosis *in vivo*.

To assess the effects of Plk inhibition on tumor growth, tumor-bearing mice were treated twice weekly with vehicle or BI-2536 for 2 weeks. As shown in Fig. 5J and K, BI-2536 dramatically inhibited tumor growth, as measured by tumor volume over time. Upon harvesting the tumors (~2.5 weeks after starting treatment), marked differences in tumor size and weight were observed (Fig. 5L and M). Overall, tumors from the BI-2536–treated mice were significantly smaller and weighed less than tumors from the vehicle-treated mice. The Aurk inhibitor PHA-739358 also blocked tumor growth and led to

Published OnlineFirst September 25, 2013; DOI: 10.1158/0008-5472.CAN-12-4258

a reduction in tumor size and weight (Supplementary Fig. S5A–S5C). Collectively, these data suggest that inhibition of G_2–M regulators can effectively block tumor progression *in vivo*.

Aurk and Plk inhibitors suppress growth of human SHH-associated medulloblastoma

The studies above focused on tumors from *patched* mutant mice. To determine whether G_2–M inhibitors might also be effective against human medulloblastoma, we used cells from patient-derived xenografts that were molecularly classified as SHH-associated medulloblastoma (Supplementary Fig. S6A and S6B). As shown in Fig. 6A, treatment of cells from the human SHH-associated medulloblastoma xenograft DMB-012 with BI-2536 caused a marked inhibition of proliferation, comparable with that seen with the SHH antagonist LDE-225. In addition, RCMB-018 cells, derived from a SHH-associated medulloblastoma that is insensitive to LDE-225 (due to amplification of SHH pathway components downstream of SMO), were also inhibited by BI-2536 (Fig. 6B). These data suggest that G_2–M inhibitors might be useful for treating human SHH-associated tumors, including those that display resistance to SHH antagonists.

To address whether Aurk inhibition and SHH pathway antagonism cooperate in human medulloblastoma, we treated DMB-012 cells with intermediate concentrations of the Aurk inhibitor PHA-739358 and the SHH antagonist LDE-225. As shown in Fig. 6C, treatment with 100 nmol/L LDE-225 alone or 100 nmol/L PHA-739358 alone caused inhibition of proliferation, as expected. However, treatment with 100 nmol/L LDE-225 together with 100 nmol/L PHA-739358 further inhibited proliferation beyond that of either compound alone. These data suggest that, similar to the results observed in cells from *patched* mutant tumors, inhibition of G_2–M regulators can cooperate with SHH pathway antagonism to block the growth of human SHH-associated medulloblastoma.

Discussion

Although treatment of medulloblastoma has significantly improved survival in recent years, patients often suffer severe side effects, and better treatment strategies are still required. Targeting medulloblastoma TPCs represents one approach to improving treatment. Using the *patched* mutant mouse (a robust model of SHH-associated medulloblastoma), we have shown that $CD15^+$ TPCs disproportionately reside in G_2–M phase of the cell cycle and that inhibition of Aurk or Plk using clinically relevant agents can inhibit tumor growth *in vitro* and *in vivo*. In addition, we have shown that these inhibitors can block the growth of cells from patient-derived xenografts of human SHH-associated medulloblastoma, including those that are resistant to SHH antagonists. Our data suggest that incorporating Aurk or Plk inhibitors into medulloblastoma therapy could lead to improvements in treatment outcome for patients with SHH-associated tumors.

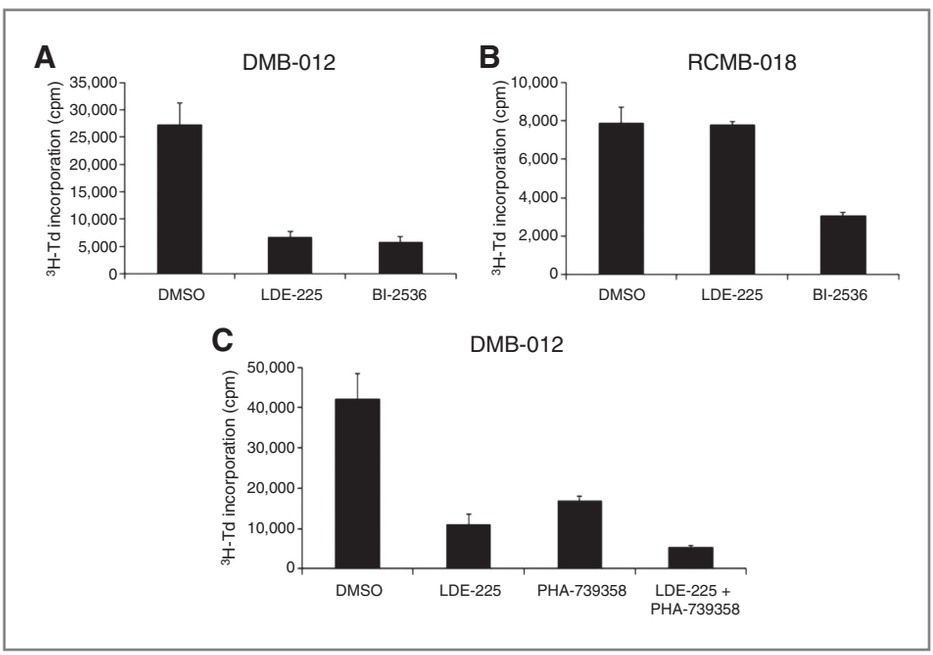

Figure 6. Aurk and Plk inhibitors suppress proliferation of human SHH-associated medulloblastoma. A and B, cells from patient-derived xenografts of SHH-associated medulloblastoma that are sensitive (DMB-012; A) or resistant (RCMB-018; B) to SHH antagonists were treated with DMSO (0.25%), LDE-225 (500 nmol/L), or BI-2536 (500 nmol/L). Cells were pulsed with ^{3}H-Td after 48 hours and harvested for analysis of ^{3}H-Td incorporation at 66 hours. In DMB-012, LDE-225 and BI-2536 significantly inhibited ^{3}H-Td incorporation compared with DMSO control ($P < 0.01$ based on paired two-tailed t test). In RCMB-018, BI-2536 caused significant inhibition ($P = 0.01$), whereas LDE-225 did not ($P = 0.89$). C, DMB-012 cells were cultured in the presence of LDE-225 (100 nmol/L), PHA-739358 (100 nmol/L), or the combination of LDE-225 + PHA-739358, and assayed for ^{3}H-Td incorporation as described earlier. Data represent means of triplicate samples ± SEM. ^{3}H-Td incorporation in the presence of LDE-225 + PHA-739358 was significantly lower than in the presence of LDE-225 alone ($P = 0.05$) or PHA-739358 alone ($P = 0.004$).

Published OnlineFirst September 25, 2013; DOI: 10.1158/0008-5472.CAN-12-4258

Our previous studies indicated that $CD15^+$ TPCs from *patched* mutant tumors display elevated expression of G_2- and M-phase cell-cycle regulators (20). Here, we confirmed increased expression of *AurkA*, *AurkB*, and *Plk1*. Each of these serine/threonine kinases plays a distinct role in G_2–M phase progression (35). AurkA is involved in centrosome duplication, bipolar spindle assembly, and entry into mitosis, whereas AurkB functions in chromatin modification, microtubule–kinetochore attachment, spindle assembly checkpoint activation, and cytokinesis. Plk1 is involved in centrosome separation, spindle assembly and maturation, cytokinesis, and exit from mitosis. Overexpression of each of these kinases has been associated with poor prognosis in multiple tumor types, leading to the notion that elevated expression of these proteins might promote tumor growth (36–42). However, given the elevated expression of multiple G_2–M regulators in $CD15^+$ cells, we hypothesized that the expression profile reflected a general property of the $CD15^+$ population, rather than a reliance on elevated expression of a single kinase to drive tumorigenicity. Cell-cycle analysis of $CD15^+$ and $CD15^-$ populations from multiple tumors demonstrated an increased percentage of the $CD15^+$ population residing in G_2–M phase compared with the $CD15^-$ population, suggesting that the elevated expression of G_2–M regulators in the $CD15^+$ population is likely a result, rather than a cause, of the increased percentage of cells residing in G_2–M.

Multiple factors could contribute to the accumulation of $CD15^+$ cells in G_2–M. One explanation is that a greater overall percentage of $CD15^+$ cells transit through the cell cycle, whereas $CD15^-$ cells remain largely stationary in G_0–G_1 phase. This notion is supported by the observation that the $CD15^+$ population also contains a greater fraction of cells in S-phase than the $CD15^-$ population. Another possible explanation for the accumulation in G_2–M could be that the $CD15^+$ cells arrest in these phases of the cell cycle. To address this possibility, we performed BrdUrd labeling and cell-cycle analysis to monitor the position of the BrdUrd-labeled cells in the cell cycle over time. We observed greater incorporation of the BrdUrd label in $CD15^+$ cells, which again suggested that greater numbers of $CD15^+$ cells transit through the cell cycle. However, examination of the BrdUrd-labeled cells over time indicated that $CD15^+$ cells do not arrest in G_2–M, but actually progress more rapidly through the cell cycle than $CD15^-$ cells. Similar results were observed using CFSE cell division analysis. Although these data do not exclude the possibility of transient checkpoint activation and/or cell-cycle arrest, they indicate that cell-cycle arrest is not a primary contributor to the over-representation of $CD15^+$ cells in G_2–M phase. Furthermore, our data suggest that both increased numbers of cycling cells and an increased pace of progression through the cell cycle contribute to the over-representation of $CD15^+$ cells in G_2–M phase.

We speculated that the increased residency of $CD15^+$ cells in G_2–M phase could represent a vulnerability of these cells that could be targeted through inhibition of G_2–M regulators. Because small-molecule inhibitors of the Aurk and Plk have shown promising efficacy in phase I and II clinical trials for other tumor types, we selected the Aurk inhibitor VX-680 and the Plk inhibitor BI-2536 for evaluation in our studies (32, 33, 43–45). Our data show that *patched* mutant tumors are indeed sensitive to Aurk or Plk inhibition; both VX-680 and BI-2536 effectively blocked proliferation *in vitro*.

One principal aim of this study was to identify approaches that might enhance current medulloblastoma therapy. SHH antagonists have recently been developed for treatment of human SHH-associated medulloblastoma (5). Both patients and mice who receive these antagonists initially respond to treatment, but they quickly develop resistance (6, 8, 46). Previous studies have shown that SHH signaling regulates the transition between the G_1 and S phases of the cell cycle (47–50); consistent with these observations, our data indicate that the SHH antagonist LDE-225 causes accumulation of cells in G_1. In contrast, the Aurk and Plk inhibitors cause accumulation in G_2–M phase. Given these distinct mechanisms of cell-cycle inhibition, we speculated that blocking G_2–M progression might represent an additional point of intervention to target the cells that escape sensitivity to SHH antagonists. Our data demonstrate that the combination of LDE-225 plus BI-2536 or VX-680 has a greater inhibitory effect than treatment with any of these compounds alone. These data suggest that clinical combination of SHH antagonists plus Aurk or Plk inhibitors might enhance the efficacy of therapy and prevent the acquired resistance to SHH antagonists.

Although the development of SHH antagonists has provided additional options for therapy, most patients with medulloblastoma are still treated with conventional chemotherapy and radiation. However, these treatments are extremely toxic and cause significant side effects (3). We questioned whether addition of Aurk or Plk inhibitors might allow for a reduction in the dose of chemo- or radiotherapy, while maintaining the efficacy of treatment. Our data show that the combination of BI-2536 or VX-680 with chemotherapeutic agents (vincristine, cisplatin, or cyclophosphamide) or radiation is more effective than chemo- or radiotherapy alone. Previous studies have shown similar effects of combined treatment of established medulloblastoma cell lines with chemo- or radiotherapy plus Aurk or Plk inhibitors (51–53). Together, these studies suggest that incorporating Aurk or Plk inhibitors into medulloblastoma therapy might enable a reduction in the doses of chemotherapy/radiotherapy and thereby reduce the long-term side-effects associated with these treatments.

The antiproliferative effects of the Aurk and Plk inhibitors *in vitro* prompted us to examine the effects of the inhibitors *in vivo*. Our data indicate that treatment of mice harboring subcutaneous allografts of *patched* mutant tumors with BI-2536 promotes apoptosis and blocks tumor growth *in vivo*. These data validate the notion that targeting a vulnerability of the TPC population using inhibitors of G_2–M regulators can block *in vivo* growth of SHH-associated tumors and suggest that inhibition of Plk may represent a viable approach for medulloblastoma treatment.

By examining the TPC population in the *patched* mutant mouse model of medulloblastoma, we have identified an opportunity for therapeutic intervention. Our data indicate that cells from patient-derived xenografts of human SHH-associated medulloblastoma are also sensitive to Aurk or Plk

Published OnlineFirst September 25, 2013; DOI: 10.1158/0008-5472.CAN-12-4258

inhibition. Importantly, tumor cells that are insensitive to SHH antagonists maintain sensitivity to BI-2536, validating the notion that treatment with the Plk inhibitor may represent an approach to overcome therapeutic resistance to SHH antagonist therapy. In addition, similar to the *patched* mutant tumor cells, treatment of human tumor cells with an Aurk inhibitor plus LDE-225 blocks proliferation more effectively than either compound alone. These data suggest that mouse and human SHH-associated medulloblastoma are sensitive to Aurk or Plk inhibition and that targeting these G_2–M regulators may represent an approach to prevent or overcome resistance to SHH antagonists. Therefore, our data strongly support the notion that incorporating Aurk or Plk inhibitors into therapeutic strategies may improve the outcome of treatment for patients with SHH-associated medulloblastoma.

Disclosure of Potential Conflicts of Interest

No potential conflicts of interest were disclosed.

Authors' Contributions

Conception and design: S.L. Markant, J.R. Crawford, R.J. Wechsler-Reya
Development of methodology: S.L. Markant, L.A. Esparza, J. Sun, L.M. McCoig, G.A. Grant, M.D. Taylor
Acquisition of data (provided animals, acquired and managed patients, provided facilities, etc.): S.L. Markant, L.A. Esparza, J. Sun, L.M. McCoig, G.A. Grant, J.R. Crawford, M.L. Levy, P.A. Northcott, M.D. Taylor
Analysis and interpretation of data (e.g., statistical analysis, biostatistics, computational analysis): S.L. Markant, G.A. Grant, P.A. Northcott, D. Shih, M. Remke, M.D. Taylor, R.J. Wechsler-Reya
Writing, review, and/or revision of the manuscript: S.L. Markant, G.A. Grant, J.R. Crawford, P.A. Northcott, M. Remke, M.D. Taylor, R.J. Wechsler-Reya
Administrative, technical, or material support (i.e., reporting or organizing data, constructing databases): L.A. Esparza, K.L. Barton, M.L. Levy
Study supervision: R.J. Wechsler-Reya

Acknowledgments

The authors thank Buddy Charbono for technical support with animal experiments, Sonja Brun, Lili Lacarra, and the Sanford-Burnham Animal Facility for help with animal colony maintenance, Beth Harvat and Mike Cook in the Duke University Flow Cytometry Core, and Jonna Hurtado, and Yoav Altman (Sanford-Burnham Flow Cytometry Shared Resource) for assistance with flow cytometry, the DNA Microarray Facility at Duke University for microarray processing, Sri Gururangan and Roger McLendon for facilitating access to patient samples, and Sandi Dunn for sharing unpublished data and helpful discussions. The authors are also grateful to Novartis for providing NVP-LDE225.

Grant Support

These studies were supported by R01-CA122759 from the National Cancer Institute (NCI) and R01 NS052323 from the National Institute of Neurological Diseases and Stroke as well as pilot funds from Golfers Against Cancer and the Pediatric Brain Tumor Foundation Institute at Duke University. R.J. Wechsler-Reya is the recipient of a Leadership Award (CIRM LA1-01747) from the California Institute for Regenerative Medicine (San Francisco, CA).

The costs of publication of this article were defrayed in part by the payment of page charges. This article must therefore be hereby marked *advertisement* in accordance with 18 U.S.C. Section 1734 solely to indicate this fact.

Received December 12, 2012; revised June 25, 2013; accepted July 2, 2013; published OnlineFirst September 25, 2013.

References

1. Merchant TE, Pollack IF, Loeffler JS. Brain tumors across the age spectrum: biology, therapy, and late effects. Semin Radiat Oncol 2010;20:58–66.
2. Crawford JR, MacDonald TJ, Packer RJ. Medulloblastoma in childhood: new biological advances. Lancet Neurol 2007;6:1073–85.
3. Pollack IF. Multidisciplinary management of childhood brain tumors: a review of outcomes, recent advances, and challenges. J Neurosurg Pediatr 2011;8:135–48.
4. Taylor MD, Northcott PA, Korshunov A, Remke M, Cho YJ, Clifford SC, et al. Molecular subgroups of medulloblastoma: the current consensus. Acta Neuropathol 2012;123:465–72.
5. Metcalfe C, de Sauvage FJ. Hedgehog fights back: mechanisms of acquired resistance against Smoothened antagonists. Cancer Res 2011;71:5057–61.
6. Rudin CM, Hann CL, Laterra J, Yauch RL, Callahan CA, Fu L, et al. Treatment of medulloblastoma with hedgehog pathway inhibitor GDC-0449. N Engl J Med 2009;361:1173–8.
7. Ramaswamy V, Northcott PA, Taylor MD. FISH and chips: the recipe for improved prognostication and outcomes for children with medulloblastoma. Cancer Genet 2011;204:577–88.
8. Buonamici S, Williams J, Morrissey M, Wang A, Guo R, Vattay A, et al. Interfering with resistance to smoothened antagonists by inhibition of the PI3K pathway in medulloblastoma. Sci Transl Med 2010;2:51ra70.
9. Al-Hajj M, Wicha MS, Benito-Hernandez A, Morrison SJ, Clarke MF. Prospective identification of tumorigenic breast cancer cells. Proc Natl Acad Sci U S A 2003;100:3983–8.
10. Singh SK, Hawkins C, Clarke ID, Squire JA, Bayani J, Hide T, et al. Identification of human brain tumour initiating cells. Nature 2004;432:396–401.
11. O'Brien CA, Pollett A, Gallinger S, Dick JE. A human colon cancer cell capable of initiating tumour growth in immunodeficient mice. Nature 2007;445:106–10.
12. Li C, Heidt DG, Dalerba P, Burant CF, Zhang L, Adsay V, et al. Identification of pancreatic cancer stem cells. Cancer Res 2007;67:1030–7.
13. Xin L, Lawson DA, Witte ON. The Sca-1 cell surface marker enriches for a prostate-regenerating cell subpopulation that can initiate prostate tumorigenesis. Proc Natl Acad Sci U S A 2005;102:6942–7.
14. Bertolini G, Roz L, Perego P, Tortoreto M, Fontanella E, Gatti L, et al. Highly tumorigenic lung cancer $CD133^+$ cells display stem-like features and are spared by cisplatin treatment. Proc Natl Acad Sci U S A 2009;106:16281–6.
15. Yang ZF, Ho DW, Ng MN, Lau CK, Yu WC, Ngai P, et al. Significance of $CD90^+$ cancer stem cells in human liver cancer. Cancer Cell 2008;13:153–66.
16. Schober M, Fuchs E. Tumor-initiating stem cells of squamous cell carcinomas and their control by TGF-beta and integrin/focal adhesion kinase (FAK) signaling. Proc Natl Acad Sci U S A 2011;108:10544–9.
17. Alison MR, Lin WR, Lim SM, Nicholson LJ. Cancer stem cells: in the line of fire. Cancer Treat Rev 2012;38:589–98.
18. Bao S, Wu Q, McLendon RE, Hao Y, Shi Q, Hjelmeland AB, et al. Glioma stem cells promote radioresistance by preferential activation of the DNA damage response. Nature 2006;444:756–60.
19. Liu G, Yuan X, Zeng Z, Tunici P, Ng H, Abdulkadir IR, et al. Analysis of gene expression and chemoresistance of $CD133^+$ cancer stem cells in glioblastoma. Mol Cancer 2006;5:67.
20. Read TA, Fogarty MP, Markant SL, McLendon RE, Wei Z, Ellison DW, et al. Identification of CD15 as a marker for tumor-propagating cells in a mouse model of medulloblastoma. Cancer Cell 2009;15:1–13.
21. Goodrich LV, Milenkovic L, Higgins KM, Scott MP. Altered neural cell fates and medulloblastoma in mouse *patched* mutants. Science 1997;277:1109–13.
22. Yang ZJ, Ellis T, Markant SL, Read TA, Kessler JD, Bourboulas M, et al. Medulloblastoma can be initiated by deletion of Patched in lineage-restricted progenitors or stem cells. Cancer Cell 2008;14:135–45.
23. Tibshirani R, Hastie T, Narasimhan B, Chu G. Diagnosis of multiple cancer types by shrunken centroids of gene expression. Proc Natl Acad Sci U S A 2002;99:6567–72.
24. Northcott PA, Shih DJ, Remke M, Cho YJ, Kool M, Hawkins C, et al. Rapid, reliable, and reproducible molecular sub-grouping of clinical medulloblastoma samples. Acta Neuropathol 2012;123:615–26.

Published OnlineFirst September 25, 2013; DOI: 10.1158/0008-5472.CAN-12-4258

25. Chen Y, Stevens B, Chang J, Milbrandt J, Barres BA, Hell JW. NS21: redefined and modified supplement B27 for neuronal cultures. J Neurosci Methods 2008;171:239–47.
26. Jensen MM, Jorgensen JT, Binderup T, Kjaer A. Tumor volume in subcutaneous mouse xenografts measured by microCT is more accurate and reproducible than determined by 18F-FDG-microPET or external caliper. BMC Med Imaging 2008;8:16.
27. Hsu JY, Sun ZW, Li X, Reuben M, Tatchell K, Bishop DK, et al. Mitotic phosphorylation of histone H3 is governed by Ipl1/aurora kinase and Glc7/PP1 phosphatase in budding yeast and nematodes. Cell 2000;102:279–91.
28. Harrington EA, Bebbington D, Moore J, Rasmussen RK, Ajose-Adeogun AO, Nakayama T, et al. VX-680, a potent and selective small-molecule inhibitor of the aurora kinases, suppresses tumor growth *in vivo*. Nat Med 2004;10:262–7.
29. Steegmaier M, Hoffmann M, Baum A, Lenart P, Petronczki M, Krssak M, et al. BI 2536, a potent and selective inhibitor of polo-like kinase 1, inhibits tumor growth *in vivo*. Curr Biol 2007;17:316–22.
30. Fink J, Sanders K, Rippl A, Finkernagel S, Beckers TL, Schmidt M. Cell type–dependent effects of Polo-like kinase 1 inhibition compared with targeted polo box interference in cancer cell lines. Mol Cancer Ther 2007;6:3189–97.
31. Miller-Moslin K, Peukert S, Jain RK, McEwan MA, Karki R, Llamas L, et al. 1-Amino-4-benzylphthalazines as orally bioavailable smoothened antagonists with antitumor activity. J Med Chem 2009;52: 3954–68.
32. Hofheinz RD, Al-Batran SE, Hochhaus A, Jager E, Reichardt VL, Fritsch H, et al. An open-label, phase I study of the polo-like kinase-1 inhibitor, BI 2536, in patients with advanced solid tumors. Clin Cancer Res 2010;16:4666–74.
33. Sebastian M, Reck M, Waller CF, Kortsik C, Frickhofen N, Schuler M, et al. The efficacy and safety of BI 2536, a novel Plk-1 inhibitor, in patients with stage IIIB/IV non–small cell lung cancer who had relapsed after, or failed, chemotherapy: results from an open-label, randomized phase II clinical trial. J Thorac Oncol 2010;5:1060–7.
34. Mross K, Frost A, Steinbild S, Hedbom S, Rentschler J, Kaiser R, et al. Phase I dose escalation and pharmacokinetic study of BI 2536, a novel Polo-like kinase 1 inhibitor, in patients with advanced solid tumors. J Clin Oncol 2008;26:5511–7.
35. Lens SM, Voest EE, Medema RH. Shared and separate functions of polo-like kinases and aurora kinases in cancer. Nat Rev Cancer 2010;10:825–41.
36. Neben K, Korshunov A, Benner A, Wrobel G, Hahn M, Kokocinski F, et al. Microarray-based screening for molecular markers in medulloblastoma revealed STK15 as independent predictor for survival. Cancer Res 2004;64:3103–11.
37. Ali HR, Dawson SJ, Blows FM, Provenzano E, Pharoah PD, Caldas C. Aurora kinase A outperforms Ki67 as a prognostic marker in ER-positive breast cancer. Br J Cancer 2012;106:1798–806.
38. Lehman NL, O'Donnell JP, Whiteley LJ, Stapp RT, Lehman TD, Roszka KM, et al. Aurora A is differentially expressed in gliomas, is associated with patient survival in glioblastoma and is a potential chemotherapeutic target in gliomas. Cell Cycle 2012;11:489–502.
39. Liang X, Wang D, Wang Y, Zhou Z, Zhang J, Li J. Expression of aurora kinase A and B in chondrosarcoma and its relationship with the prognosis. Diagn Pathol 2012;7:84.
40. Lin ZZ, Jeng YM, Hu FC, Pan HW, Tsao HW, Lai PL, et al. Significance of Aurora B overexpression in hepatocellular carcinoma. Aurora B overexpression in HCC. BMC Cancer 2010;10:461.
41. King SI, Purdie CA, Bray SE, Quinlan PR, Jordan LB, Thompson AM, et al. Immunohistochemical detection of Polo-like kinase-1 (PLK1) in primary breast cancer is associated with TP53 mutation and poor clinical outcome. Breast Cancer Res 2012;14:R40.
42. Cheng MW, Wang BC, Weng ZQ, Zhu XW. Clinicopathological significance of Polo-like kinase 1 (PLK1) expression in human malignant glioma. Acta Histochem 2012;114:503–9.
43. Cheung CH, Coumar MS, Chang JY, Hsieh HP. Aurora kinase inhibitor patents and agents in clinical testing: an update (2009–10). Expert Opin Ther Pat 2011;21:857–84.
44. Chopra P, Sethi G, Dastidar SG, Ray A. Polo-like kinase inhibitors: an emerging opportunity for cancer therapeutics. Expert Opin Investig Drugs 2010;19:27–43.
45. Traynor AM, Hewitt M, Liu G, Flaherty KT, Clark J, Freedman SJ, et al. Phase I dose escalation study of MK-0457, a novel aurora kinase inhibitor, in adult patients with advanced solid tumors. Cancer Chemother Pharmacol 2011;67:305–14.
46. Yauch RL, Dijkgraaf GJ, Alicke B, Januario T, Ahn CP, Holcomb T, et al. Smoothened mutation confers resistance to a Hedgehog pathway inhibitor in medulloblastoma. Science 2009;326:572–4.
47. Adolphe C, Hetherington R, Ellis T, Wainwright B. Patched1 functions as a gatekeeper by promoting cell cycle progression. Cancer Res 2006;66:2081–8.
48. Cayuso J, Ulloa F, Cox B, Briscoe J, Marti E. The Sonic hedgehog pathway independently controls the patterning, proliferation and survival of neuroepithelial cells by regulating Gli activity. Development 2006;133:517–28.
49. Kenney AM, Rowitch DH. Sonic hedgehog promotes G(1) cyclin expression and sustained cell cycle progression in mammalian neuronal precursors. Mol Cell Biol 2000;20:9055–67.
50. Oliver TG, Grasfeder LL, Carroll AL, Kaiser C, Gillingham CL, Lin SM, et al. Transcriptional profiling of the Sonic hedgehog response: a critical role for N-myc in proliferation of neuronal precursors. Proc Natl Acad Sci U S A 2003;100:7331–6.
51. Muscal JA, Scorsone KA, Zhang L, Ecsedy JA, Berg SL. Additive effects of vorinostat and MLN8237 in pediatric leukemia, medulloblastoma, and neuroblastoma cell lines. Invest New Drugs 2012;31:39–45.
52. Harris PS, Venkataraman S, Alimova I, Birks DK, Donson AM, Knipstein J, et al. Polo-like kinase 1 (PLK1) inhibition suppresses cell growth and enhances radiation sensitivity in medulloblastoma cells. BMC Cancer 2012;12:80.
53. El-Sheikh A, Fan R, Birks D, Donson A, Foreman NK, Vibhakar R. Inhibition of aurora kinase A enhances chemosensitivity of medulloblastoma cell lines. Pediatr Blood Cancer 2010;55:35–41.
54. Northcott PA, Korshunov A, Witt H, Hielscher T, Eberhart CG, Mack S, et al. Medulloblastoma comprises four distinct molecular variants. J Clin Oncol 2011;29:1408–14.